

Simulation of the Einstein–de Haas effect combining molecular and spin dynamics

W. Dednam^{a,b,*}, C. Sabater^b, A. E. Botha^a, E. B. Lombardi^a, J. Fernández-Rossier^c, M. J. Caturla^b

^a*Department of Physics, Unisa Science Campus, University of South Africa, Johannesburg 1710, South Africa*

^b*Departamento de Física Aplicada and Unidad asociada CSIC, Universidad de Alicante, Campus de San Vicente del Raspeig, E-03690 Alicante, Spain.*

^c*International Iberian Nanotechnology Laboratory, 4715-310 Braga, Portugal*

Abstract

The spin and lattice dynamics of a ferromagnetic nanoparticle are studied via molecular dynamics and with semi-classical spin dynamics simulations where spin and lattice degrees of freedom are coupled via a dynamic uniaxial anisotropy term. We show that this model conserves total angular momentum, whereas spin and lattice angular momentum are not conserved. We carry out simulations of the the Einstein–de Haas effect for a Fe nanocluster with more than 500 atoms that is free to rotate, using a modified version of the open-source spin-lattice dynamics code (SPILADY). We show that the rate of angular momentum transfer between spin and lattice is proportional to the strength of the magnetic anisotropy interaction. The addition of the anisotropy allows full spin-lattice relaxation to be achieved on previously reported timescales of ~ 100 ps and for tight-binding magnetic anisotropy energies comparable to those of small Fe nanoclusters.

Keywords: Spin-lattice dynamics, Molecular dynamics simulations, Magnetic anisotropy, Conservation of total angular momentum, Angular momentum exchange, Einstein–de Haas effect

*Corresponding author

Email address: dednaw@unisa.ac.za (W. Dednam)

1. Introduction

First observed by Einstein and De Haas [1] in 1915, the so-called Einstein–de Haas (EdH) effect involves the rotation of a magnetic object through change in its magnetization. The converse effect, i.e. magnetization through a rotational change, was discovered contemporaneously by Barnett [2]. Both effects rely on the conservation of the total angular momentum and are governed by the same gyromagnetic tensor components, satisfying the Onsager reciprocal relations [3–5]. Thus, for any particular physical system, experimental confirmation of either effect is thought to be sufficient to establish conservation of total angular momentum [6]. Arguably, the EdH effect is more widely known because of its routine use in measuring the g factors of various ferromagnetic materials: Fe, Co, Ni, etc. [7]. Recently, the EdH effect has also been observed in a ferromagnetic thin film, deposited on a microcantilever [8].

Despite several theoretical studies [10–13], a microscopic description of the two effects, either in terms of computer simulations or theoretically, remains a challenging and open problem. On the theoretical front the most recent work by Mentink *et al.* [13] shows that, to accurately determine the timescale of angular momentum exchange between electronic and lattice degrees of freedom, and to establish whether the exchange is local or non-local, it is necessary to cast both quantum subsystems in the angular momentum representation. In practice, this involves “dressing” every atom with phonons that exchange angular momentum locally with the multi-electron atom’s spins and electronic orbital angular momenta. The quantum many-body Hamiltonian obtained in this way is fully rotationally invariant and a static non-perturbative variational calculation shows that phonons quench the electronic orbital angular momentum of the atoms as the coupling strength between the lattice and electronic degrees of freedom increases. A dynamic non-perturbative variational calculation by the same authors [13], on the other hand, reveals the emergence of high frequency peaks in the magnetic susceptibility as the electron-phonon coupling strength increases. These peaks are consistent with the timescale of the ultra-fast EdH ef-

fect that was observed recently in experiments of laser-induced demagnetization in an isolated ferromagnetic sample [38].

Transfer of angular momentum between spin and motional degrees of freedom ultimately occurs due to spin-orbit interactions that couple these degrees of freedom. In the spin-lattice dynamics (SLD) model, spin-orbit interactions lead to magnetic anisotropy terms that depend explicitly on the atomic positions, thereby coupling spin and lattice degrees of freedom [9, 15–22]. Importantly, total angular momentum must be conserved.

In this work we implement the SLD model of Ref. [17]. The model is based on a truncated Taylor expansion of the magnetic anisotropy energy [23]. We demonstrate that it is able to reproduce spin-lattice relaxation times ~ 100 ps, consistent with previously reported values [15, 17, 20]. Our implementation of the SLD model is applicable to combined molecular and spin dynamics of systems of arbitrary symmetry (including bulk, clusters, defect systems, etc.) It allows the modelling of a wide range of potential new systems at finite temperatures, for example: non-collinear magnetic domain walls in ferromagnetic atomic-sized contacts or wires [24–26], chiral spin textures in magnetic nanoparticles [27, 28], skyrmions [29, 30], and an atomistic description of the Barnett [2] and Barkhausen [31] effects, amongst others.

The remaining material is organized as follows. In Section 2, we give a brief outline of the SLD model of ferromagnetic exchange previously implemented in SPILADY [32] and demonstrate analytically that it conserves angular momentum. However, we show that angular momentum exchange is not possible when only the isotropic ferromagnetic exchange term is considered in the model. We therefore show analytically in Section 2 that, by adding the second-order anisotropy correction of Ref. [17] to the SLD model, not only is total angular momentum conserved, but also exchange of angular momenta between spin and lattice is facilitated. In Section 3, we discuss our choice of semi-classical potentials and parameters to perform SLD simulations of ferromagnetic iron nanoclusters and then demonstrate numerically that our implementation replicates the Einstein–de Haas effect in a small iron nanocluster. Finally, we conclude the paper by

summarizing our findings in Section 4.

2. Models and analytical considerations

2.1. General description of the SLD model

Our implementation builds on the well-established technique known as spin-lattice dynamics (SLD) [9, 15, 20, 32, 33]. This is a semi-classical molecular dynamics approach which allows the simultaneous evolving of atomic spin and position degrees of freedom. The atom-atom interactions in this model are described by the widely-used embedded atom method (EAM) potential [34]. The EAM potential has been implemented in SPILADY [32, 33] along with a generalized Heisenberg model of ferromagnetic exchange:

$$H = \sum_i^N \frac{\vec{p}_i^2}{2m} + V + H_{spin} \quad (1)$$

In Eq. (1), \vec{p}_i is the momentum operator for the i th atom and V is the interatomic EAM potential energy function that models the basic interactions between the atoms, i.e. excluding the spin interactions. Expressed in terms of the spin angular momentum vectors of particles i and j , the spin Hamiltonian H_{spin} is a sum of the Zeeman term (H_{Zeeman}), the generalized Heisenberg exchange term (H_{exch}) and the anisotropy term (H_{anis}):

$$H_{spin} = H_{Zeeman} + H_{exch} + H_{anis} \quad (2)$$

with

$$H_{Zeeman} = - \sum_i \vec{M}_i \cdot \vec{B}_{ext} = \sum_i g\mu_B \vec{S}_i \cdot \vec{B}_{ext}, \quad (3)$$

and

$$H_{exch} = -\frac{1}{2} \sum_i J_{ij}(r_{ij}) \left[\vec{S}_i \cdot \vec{S}_j - \left| \vec{S}_i \right| \left| \vec{S}_j \right| \right]. \quad (4)$$

The anisotropy term, H_{anis} , is discussed in the next section. The Zeeman term in Eq. (3) is due to an external magnetic field \vec{B}_{ext} , where $\vec{M}_i = -g\mu_B \vec{S}_i$ is the magnetic dipole moment, $g = 2.002319$ is the electron's gyromagnetic factor

and μ_B is the Bohr magneton. The exchange term, Eq. (4), is isotropic in form, with $r_{ij} = |\vec{r}_i - \vec{r}_j|$ being the magnitude of the displacement $\vec{r}_{ij} = \vec{r}_i - \vec{r}_j$ between the i th and j th atoms. \vec{S}_i is the (dimensionless) atomic spin or spin angular momentum vector at site i and the quantities $J_{ij}(r_{ij})$ are obtained from a shifted fitting function of the form [17, 33]

$$J_{ij}(r_{ij}) = J_0 (1 - r_{ij}/r_c)^3 \Theta(r_c - r_{ij}), \quad (5)$$

in which J_0 is the only fitting parameter, $\Theta(r_c - r_{ij})$ is the Heavyside step function, and r_c is the cut-off radius.

Next, we discuss the conservation of total angular momentum in the Heisenberg model of ferromagnetic exchange implemented in SPILADY.

2.2. Conservation of total angular momentum in SLD simulations

We briefly revisit the textbook derivation of angular momentum conservation in a system of classical particles. We define the total angular momentum of a system of classical particles:

$$\vec{L} = \sum_i \vec{L}_i \quad (6)$$

where $\vec{L}_i = m_i \vec{r}_i \times \vec{v}_i$ is the angular momentum of an individual particle. The rate of change of the total angular momentum is governed by the following equation:

$$\frac{d\vec{L}}{dt} = \sum_i \frac{d\vec{L}_i}{dt} = \sum_i \vec{r}_i \times \vec{F}_i \quad (7)$$

We can break down the force acting on particle i into two parts, the forces coming from external sources outside of the system and the internal forces, $\vec{F}_i = (\vec{F}_{i,\text{ext}} + \vec{F}_{i,\text{int}})$, where the internal forces are given by

$$\vec{F}_{i,\text{int}} = \sum_{j \neq i} \vec{f}_{ji} \quad (8)$$

and where \vec{f}_{ji} is the force that particle j exerts on i . By Newton's third law, $\vec{f}_{ji} = -\vec{f}_{ij}$. Therefore, for any pair of particles i and j , the contributions to the

rate of change of the angular momentum deriving from their mutual interaction only, are:

$$\left. \frac{d\vec{L}_i}{dt} \right|_{\text{int},j} + \left. \frac{d\vec{L}_j}{dt} \right|_{\text{int},i} = \vec{r}_i \times \vec{f}_{ji} + \vec{r}_j \times \vec{f}_{ij} = (\vec{r}_i - \vec{r}_j) \times \vec{f}_{ji} \quad (9)$$

Now, if the internal forces \vec{f}_{ij} are central, then they do not contribute to the rate of change of angular momentum of the system, and we are left with only the external forces. Moreover, a force $\vec{f}_{ij} = -\vec{\nabla}U(|\vec{r}_i - \vec{r}_j|)$ that can be obtained as a gradient of a potential U , such as the EAM potential [34] used in this work, is automatically central and, by virtue of being expressed as a gradient of a scalar function, conservative.

This shows that, for an isolated system of classical particles, in the absence of external forces, and with internal forces that are central, the rotational angular momentum is conserved.

Equation (3) shows that the atomic spins in our implementation are dimensionless. Consequently, in order to calculate the dimensionless classical angular momentum, we define $\vec{\lambda} = \frac{\vec{L}}{\hbar}$ with $\hbar = 6.58211899 \times 10^{-16}$ eV.s in the following expressions involving the classical angular momentum. So, substituting the Heisenberg exchange term, Eq. (4), into Eq. (9) yields for the rate of change of the lattice angular momentum:

$$\begin{aligned} \left. \frac{d\vec{\lambda}_i}{dt} \right|_{\text{exch},j} + \left. \frac{d\vec{\lambda}_j}{dt} \right|_{\text{exch},i} &= \frac{1}{\hbar} \left[\vec{r}_i \times \vec{f}_{ji} + \vec{r}_j \times \vec{f}_{ij} \right] = \frac{1}{\hbar} \left[\vec{r}_i \times -\vec{\nabla}_i H_{\text{exch},j} + \vec{r}_j \times -\vec{\nabla}_j H_{\text{exch},i} \right] \\ &= -\vec{r}_i \times \frac{1}{\hbar r_{ij}} \frac{dJ_{ij}(r_{ij})}{dr_{ij}} \left[\vec{S}_i \cdot \vec{S}_j - |\vec{S}_i| |\vec{S}_j| \right] \vec{r}_{ij} + \vec{r}_j \times \frac{1}{\hbar r_{ji}} \frac{dJ_{ji}(r_{ji})}{dr_{ji}} \left[\vec{S}_j \cdot \vec{S}_i - |\vec{S}_j| |\vec{S}_i| \right] \vec{r}_{ij} \\ &= (-\vec{r}_i + \vec{r}_j) \times \frac{1}{\hbar r_{ij}} \frac{dJ_{ij}(r_{ij})}{dr_{ij}} \left[\vec{S}_i \cdot \vec{S}_j - |\vec{S}_i| |\vec{S}_j| \right] \vec{r}_{ij} \\ &= \frac{1}{\hbar r_{ij}} \frac{dJ_{ij}(r_{ij})}{dr_{ij}} \left[\vec{S}_i \cdot \vec{S}_j - |\vec{S}_i| |\vec{S}_j| \right] \vec{r}_{ij} \times \vec{r}_{ij} = 0 \end{aligned} \quad (10)$$

We therefore see that the classical or rotational angular momentum is conserved in an isotropic model of ferromagnetic exchange.

With a view to establishing conservation of spin angular momentum in SLD

models, we need to derive an expression analogous to Eq. (9) involving the rates of change of the angular momentum of spins i and j . To that end, we start with the equation of motion for the classical spin momentum of particle i :

$$\frac{d\vec{S}_i}{dt} = -\vec{S}_i \times \frac{1}{\hbar} \nabla_{\vec{S}_i} H_{\text{spin}} \quad (11)$$

where the energy of the spin system, H_{spin} , is in general a function of \vec{S}_i , \vec{S}_j and of the coordinates of the atoms and their velocities.

We first compute the effective field associated with the first two terms of Eq. (2), classically. For the first term, H_{Zeeman} , we obtain:

$$\nabla_{\vec{S}_i} H_{\text{Zeeman}} = g\mu_B \vec{B}_i \quad (12)$$

This term produces a rate of change of the spin momentum when \vec{S}_i is not parallel to \vec{B}_i , and, consequently, we do not consider total angular momentum conservation in the presence of an external magnetic field any further.

The second term, H_{exch} , produces central forces when we compute the associated gradients. Since individual spin magnitudes are conserved in our model, we have for the spin torques:

$$\nabla_{\vec{S}_i} H_{\text{exch}} = -\frac{1}{2} \sum_j J(r_{ij}) \vec{S}_j \quad (13)$$

By analogy with Eq. (9), we find that for any pair of particles i and j the contribution to the rate of change of the spin angular momentum coming from this term vanishes:

$$\left. \frac{d\vec{S}_i}{dt} \right|_{\text{exch},j} + \left. \frac{d\vec{S}_j}{dt} \right|_{\text{exch},i} = \frac{J(r_{ij})}{\hbar} \left(\vec{S}_i \times \vec{S}_j + \vec{S}_j \times \vec{S}_i \right) = 0 \quad (14)$$

In other words, isotropic interactions of the scalar form $\vec{S}_1 \cdot \vec{S}_2$ preserve the spin angular momentum pairwise.

Therefore, the Heisenberg model of ferromagnetic exchange in Eq. (4) not only conserves total angular momentum, but does so separately within the spin

and lattice sub-reservoirs, and cannot account for angular momentum transfer between lattice and spin degrees of freedom.

In the next section, we consider the correction H_{anis} , which couples the spin and lattice degrees of freedom, allowing transfer of angular momentum between spin and lattice, while still conserving total angular momentum.

2.3. Addition of magnetic anisotropy

To permit exchange of angular momentum between spins and lattice, we have implemented in the SPILADY code [32] the model of anisotropy described in Ref. [17]. We exclude the first-order anisotropy correction of Ref. [17] since it does not preserve time-reversal symmetry in the absence of an external field. Therefore we only consider the second-order (uniaxial) anisotropy correction of Ref. [17] in our implementation:

$$H_{\text{anis}} = -C_2 \sum_{i,\alpha,\beta} S_\alpha(i) \Lambda_{\alpha,\beta}(i) S_\beta(i), \quad (15)$$

In Eq. (15), $\Lambda_{\alpha,\beta}(i) = \frac{\partial^2 \rho_i(r_{ij})}{\partial x_{i\alpha} \partial x_{i\beta}}$, with $\alpha, \beta = 1, 2, 3$ Cartesian components, is the Hessian matrix element with respect to lattice site i , of the semi-classical *many-body*, EAM electron density-like, function:

$$\rho_i(r_{ij}) = \begin{cases} \sum_{j \neq i} \left(1 - \frac{r_{ij}}{r_0}\right)^4 e^{\left(1 - \frac{r_{ij}}{r_0}\right)} & r_{ij} \leq r_0 \\ 0 & r_{ij} > r_0, \end{cases} \quad (16)$$

where r_0 is the cut-off distance between second and third nearest neighbours and C_2 is a proportionality constant which determines the relative strength of the anisotropy term [17].¹

Thus, the contribution of the anisotropy to the effective local magnetic field at atom i from neighbouring spins within the cut-off r_0 becomes:

$$\nabla_{\vec{S}_i} H_{\text{anis}} = -C_2 \sum_{j \neq i} \left[g(r_{ij}) \vec{S}_i + \frac{1}{r_{ij}} \frac{dg(r_{ij})}{dr_{ij}} (\vec{r}_{ij} \cdot \vec{S}_i) \vec{r}_{ij} \right] \quad (17)$$

¹The interested reader is referred to Ref. [35] for full details of our implementation in SPILADY of the algorithms described in Refs. [16, 17, 36, 37].

where $g(r_{ij}) = \frac{1}{r_{ij}} \frac{d\phi(r_{ij})}{dr_{ij}}$ with $r_{ij} = |\vec{r}_i - \vec{r}_j|$ and $\phi(r_{ij})$ is the expression under the summation in Eq. (16).

Evaluating $\frac{d\vec{S}_i}{dt} = -\vec{S}_i \times \frac{1}{\hbar} \nabla_{\vec{S}_i} H_{\text{anis}}$ for the spin at site i yields

$$\frac{d\vec{S}_i}{dt} = \frac{C_2}{\hbar} \sum_{k \neq i} \left[\frac{1}{r_{ik}} \frac{dg(r_{ik})}{dr_{ik}} (\vec{r}_{ik} \cdot \vec{S}_i) \vec{S}_i \times \vec{r}_{ik} \right] \quad (18)$$

In the same way, for the spin at site j ,

$$\frac{d\vec{S}_j}{dt} = \frac{C_2}{\hbar} \sum_{k \neq j} \left[\frac{1}{r_{jk}} \frac{dg(r_{jk})}{dr_{jk}} (\vec{r}_{jk} \cdot \vec{S}_j) \vec{S}_j \times \vec{r}_{jk} \right] \quad (19)$$

Finally, for the j th term from $\frac{d\vec{S}_i}{dt}$ and the i th term from $\frac{d\vec{S}_j}{dt}$, summing gives

$$\left. \frac{d\vec{S}_i}{dt} \right|_j + \left. \frac{d\vec{S}_j}{dt} \right|_i = \frac{C_2}{\hbar r_{ij}} \frac{dg(r_{ij})}{dr_{ij}} \left[(\vec{r}_{ij} \cdot \vec{S}_i) \vec{S}_i \times \vec{r}_{ij} + (\vec{r}_{ij} \cdot \vec{S}_j) \vec{S}_j \times \vec{r}_{ij} \right] \quad (20)$$

since two instances of $\vec{r}_{ji} = -\vec{r}_{ij}$ occur in the second term so their minus signs cancel when the indices of i and j are swapped.

Next, we consider the lattice torque term, showing that it exactly compensates the spin torque term of Eq. (20).

The expression for the ‘‘anisotropy’’ force on the spin at site i due to all neighbours j within the cut-off of Eq. (16) is:

$$\begin{aligned} \vec{f}_{\text{anis},i} &= \frac{1}{2} C_2 \sum_{j \neq i} \frac{1}{r_{ij}} \left[\frac{dg(r_{ij})}{dr_{ij}} \{ \vec{S}_i \cdot \vec{S}_i + \vec{S}_j \cdot \vec{S}_j \} \vec{r}_{ij} \right. \\ &\quad \left. - \frac{dg(r_{ij})}{dr_{ij}} \left\{ \frac{(\vec{r}_{ij} \cdot \vec{S}_i)^2}{r_{ij}^2} - \frac{(\vec{r}_{ij} \cdot \vec{S}_j)^2}{r_{ij}^2} \right\} \vec{r}_{ij} \right. \\ &\quad \left. + 2 \frac{dg(r_{ij})}{dr_{ij}} \{ (\vec{r}_{ij} \cdot \vec{S}_i) \vec{S}_i + (\vec{r}_{ij} \cdot \vec{S}_j) \vec{S}_j \} \right. \\ &\quad \left. + \frac{1}{r_{ij}} \frac{d^2g(r_{ij})}{d^2r_{ij}} \left\{ (\vec{r}_{ij} \cdot \vec{S}_i)^2 + (\vec{r}_{ij} \cdot \vec{S}_j)^2 \right\} \vec{r}_{ij} \right] \end{aligned} \quad (21)$$

Then, by substituting Eq. (21) into (9), and considering only the pair of

particles i and j , we obtain after some algebra,

$$\begin{aligned} \left. \frac{d\vec{\lambda}_i}{dt} \right|_j + \left. \frac{d\vec{\lambda}_j}{dt} \right|_i &= \frac{1}{\hbar} \vec{r}_{ij} \times \vec{f}_{ji} \\ &= \frac{C_2}{\hbar r_{ij}} \frac{dg(r_{ij})}{dr_{ij}} \left[(\vec{r}_{ij} \cdot \vec{S}_i) \vec{r}_{ij} \times \vec{S}_i + (\vec{r}_{ij} \cdot \vec{S}_j) \vec{r}_{ij} \times \vec{S}_j \right], \end{aligned} \quad (22)$$

where we have used the fact that the cross product of a vector with itself is zero.

Clearly, Eqs. (20) and (22) compensate each other when the cross products are commuted in Eq. (22) to appear in the same order as in Eq. (20). We have therefore shown analytically that the model of Ref. [17] permits exchange of angular momentum, while at the same time guaranteeing conservation of total angular momentum.

3. Numerical simulation results

We validate our implementation of the anisotropy correction by studying the phenomenon known as the Einstein–de Haas effect [1]. In its simplest version, the EdH experiment involves using a strong magnetic field to change the magnetization of a small freely suspended cylinder made of a ferromagnetic material. The sudden change in magnetization in the cylinder brought on by the strong magnetic field then manifests as a physical rotation about the axis of the sample as it evolves towards a new equilibrium magnetization due to the conservation of the total (spin + rotational) angular momentum. The effect is well-known, but its microscopic origin has only been recently demonstrated in ultrafast (femtosecond scale) laser-induced demagnetization experiments [38], though in that particular case the electronic degrees of freedom are also involved since the laser primarily excites the electrons [39, 40].

3.1. Simulation parameters for Fe

In our numerical simulations of the EdH effect, we use a small prolate spheroid made of iron. We choose this shape because the anisotropy is uniaxial and a positive value of C_2 will see the spins aligning preferentially along the long axis of the spheroid. It consists of 505 Fe atoms cut out from a bulk

periodic simulation cell of body-centered cubic (BCC) Fe(001). The particle is perfectly symmetric about its central axis along the z direction, i.e., the x and y components of each of its constituent atoms sum to 0 with respect to this axis.

To describe the interatomic interactions, we use the Malerba et al. [41] EAM potential with a per-atom cohesive energy of -4.122 eV/atom. This contrasts with the 0 eV cohesive energy of the Harmonic and Morse potentials used in Refs. [9, 22]. The EAM potential used in this work is more realistic in that it is able to more accurately reproduce material properties [41], including defects and the *ab-initio* energy of a free Fe(001) surface.

Then, for the Heisenberg exchange term in Eq. (4), we employ the same parameter values as in Table II of Ref. [22]: $J_0 = 0.904$ eV and $r_c = 3.75$ Å.

Finally, for the anisotropy term in Eq. (15), we use $C_2 = 0.025$ eV.Å² and $r_0 = 3.5$ Å.² This value of C_2 has been estimated by determining the difference in magnetic anisotropy energy (MAE) of the relaxed spheroid, with spins and atoms frozen, compared to the MAE with spins perpendicular to the first configuration, resulting in $\Delta\text{MAE} \sim 0.2$ meV/atom, in good agreement with the value of ~ 0.2 meV/atom reported in Fig. 7 of Ref. [42] for a similar-sized Fe nanocluster using a tight-binding formalism.³

3.2. SLD simulation of the Einstein-de Haas effect

We simulate the EdH effect by mirroring an experiment where an initially demagnetized sample (such as via heat shock) is allowed to relax to an equilibrium magnetized state, while observing the rotational angular momentum which

²We have discovered that the units of C_1 and C_2 are quoted incorrectly in Ref. [17], since they should be eV.Å and eV.Å², respectively.

³We note that our implementation does not model the weak static background anisotropy of $3d$ transition metals, which, for example, gives rise to their preferred bulk magnetic easy axes. Rather, it accounts for dynamic anisotropy due to local symmetry-breaking about a given lattice site that may dominate at sufficiently high temperatures approaching the Debye temperature of the metal [23]. Nevertheless, dynamic many-body effects, such as those used in this model, play an important role [13] in fast demagnetization processes in ferromagnetic materials that cannot be modelled by static background anisotropy alone.

is induced by spins flipping and precessing as the sample reaches its equilibrium magnetization.

We therefore use an input configuration for our SLD simulation which consists of fully randomized spins, as shown in Fig. 1 (a). The sample is then allowed to relax for a period of 1 ns, reaching an equilibrium magnetized state after ~ 100 ps, as illustrated in Fig. 1 (b), where we see the spins have mostly aligned parallel to the easy axis.⁴

In Fig. 1 (c) we plot the time evolution of the average per-atom spin and rotational angular momentum for $C_2 = 0.025 \text{ eV}\cdot\text{\AA}^2$. Both the rotational lattice and spin angular momenta are initially near 0. As the simulation proceeds, angular momentum is transferred from the spins as they rotate (during the process of reaching a final equilibrium magnetized state), to rotational lattice angular momentum, while conserving the total angular momentum. The magnitude of the total average angular momentum, or red line, in Fig. 1 (c) has been calculated as

$$\left| \langle \vec{\lambda} + \vec{S} \rangle \right| = \left([\langle \lambda_x \rangle + \langle S_x \rangle]^2 + [\langle \lambda_y \rangle + \langle S_y \rangle]^2 + [\langle \lambda_z \rangle + \langle S_z \rangle]^2 \right)^{1/2}. \quad (23)$$

We note that the average per atom spin angular momentum of $\sim 0.8 \left| \vec{S} \right|_{\text{initial}}$ is higher than expected at the temperature⁵ of ~ 500 K shown in Fig. 1 (d), due to the model of Refs. [17, 22, 33] which does not account for size dependence of magnetization in nanoparticles [44, 45].

In Fig. 2 (a) we plot the difference in magnetic anisotropy energy ΔMAE of the spin populations at 90° to one another as a function of C_2 ; it is seen that ΔMAE is linear in C_2 , verifying that the MAE is directly proportional to C_2 .

⁴See Supplemental Material at <http://link.xxx.org/supplemental/xxxx/xxxx.xxx> for movies of the atoms and spins of the spheroid in Fig. 1 for $C_2 = 0.025, 0.05, 0.075, 0.1, 0.15$ and $0.2 \text{ eV}\cdot\text{\AA}^2$ showing how the nanocluster evolves to the final states depicted in Fig. 1

⁵SPILADY calculates the lattice temperature from the equipartition of kinetic energy in three dimensions and we implemented the generalized expression for the spin temperature developed by Nurdin et al. [43] in SPILADY.

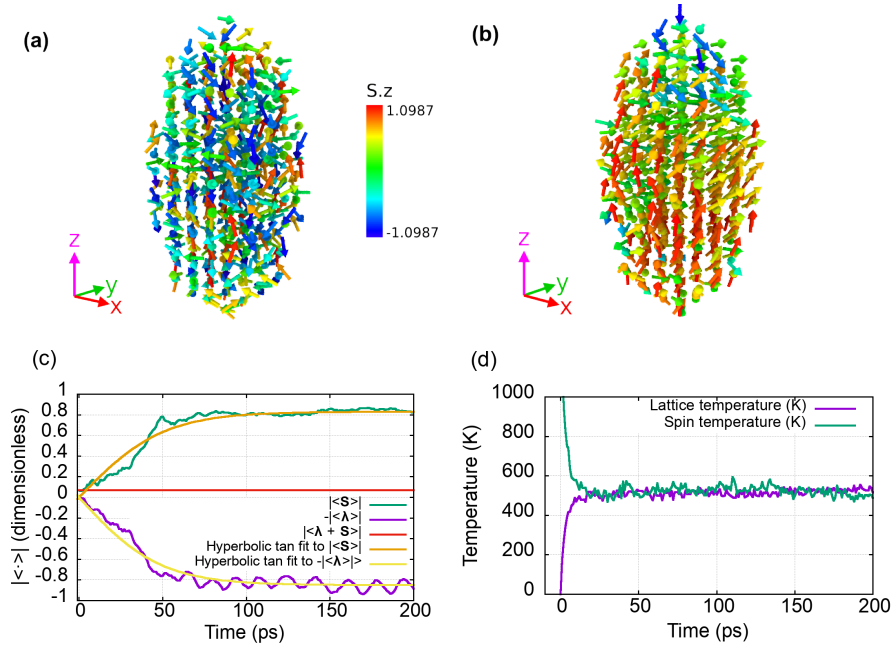


Figure 1: (a) Initial ($t = 0$) spin configuration of the Fe(001) prolate spheroid. The atoms (not shown) are placed near the sites they would occupy in a perfectly ordered BCC lattice of Fe(001) and the spins are initially randomly oriented. (b) After $t = 100$ ps, the spins mostly point upward. The color legend refers to the magnitude of the (dimensionless) atomic spins on the positive z -axis, i.e., the direction of saturation magnetization of Fe, $2.2\mu_B$, divided by the electron's gyromagnetic factor, $g = 2.002319$, and $1.0\mu_B$. (c) Conservation of total average per-atom angular momentum (red) as a sum of contributions from the atomic spins $|\langle \vec{S} \rangle|$ (green) and lattice $-\langle \vec{\lambda} \rangle$ (purple) for $C_2 = 0.025 \text{ eV}\cdot\text{\AA}^2$. For convenience, the negative of $|\langle \vec{\lambda} \rangle|$ has been plotted so that $|\langle \vec{S} \rangle|$ coincides with the general orientation of $\langle \vec{S} \rangle$ in (b). Hyperbolic tangent fits to $|\langle \vec{S} \rangle|$ (orange) and $-\langle \vec{\lambda} \rangle$ (yellow) are also shown. (d) The lattice temperature (purple), initially 0 K, rises rapidly while the spin temperature (green), initially ~ 12000 K, converges equally rapidly to the equilibrium temperature of ~ 500 K for $C_2 = 0.025 \text{ eV}\cdot\text{\AA}^2$.

Further, we verify that the strength of the anisotropy correction C_2 determines the rate of exchange of angular momentum between spins and lattice rotational angular momentum. To this end, and for ease of comparison, we fit the absolute values of the average per-atom lattice and spin angular momenta to the hyperbolic tangent function $a \tanh(bt)$ using the first 500 ps of simula-

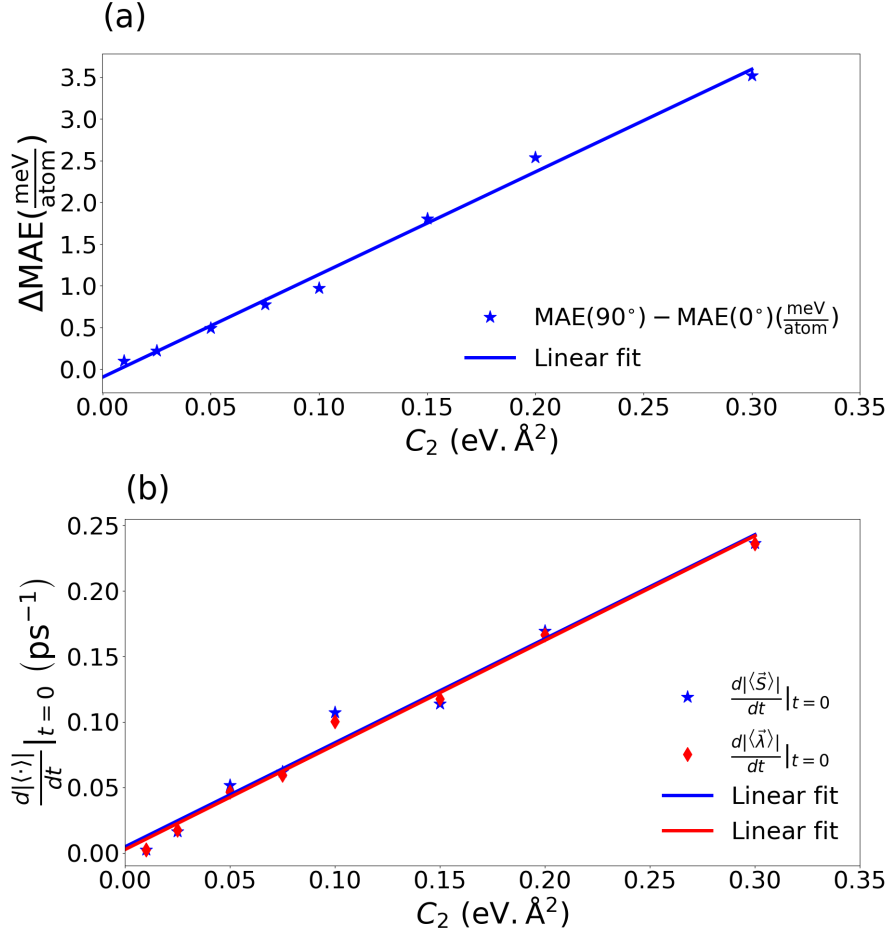


Figure 2: (a) The magnetic anisotropy energy difference scales linearly with C_2 ($R^2 = 0.993$) and the range of ΔMAE values are ~ 1 meV/atom [42]. (b) The dependence on C_2 of the rate of change in angular momentum is clear, with stronger anisotropic interactions (larger C_2) resulting in more rapid change in angular momenta. (Here, $R^2 = 0.978$ in the case of the spins and 0.988 in the case of the lattice.)

tion data in each case, as illustrated in Fig. 1 (c) for the particular case of $C_2 = 0.025$ $\text{eV} \cdot \text{\AA}^2$. The rate of change of angular momentum is the greatest near the origin; therefore we use the derivatives of the fits to this function at $t = 0$ as measure of the rate of exchange of angular momentum. In Fig. 2 (b) we plot the rates of change of spin and lattice rotational angular momenta as

a function of C_2 . It is seen that the rate of exchange of angular momenta is linear in C_2 , verifying that this rate is directly proportional to the strength of the magnetic anisotropy.

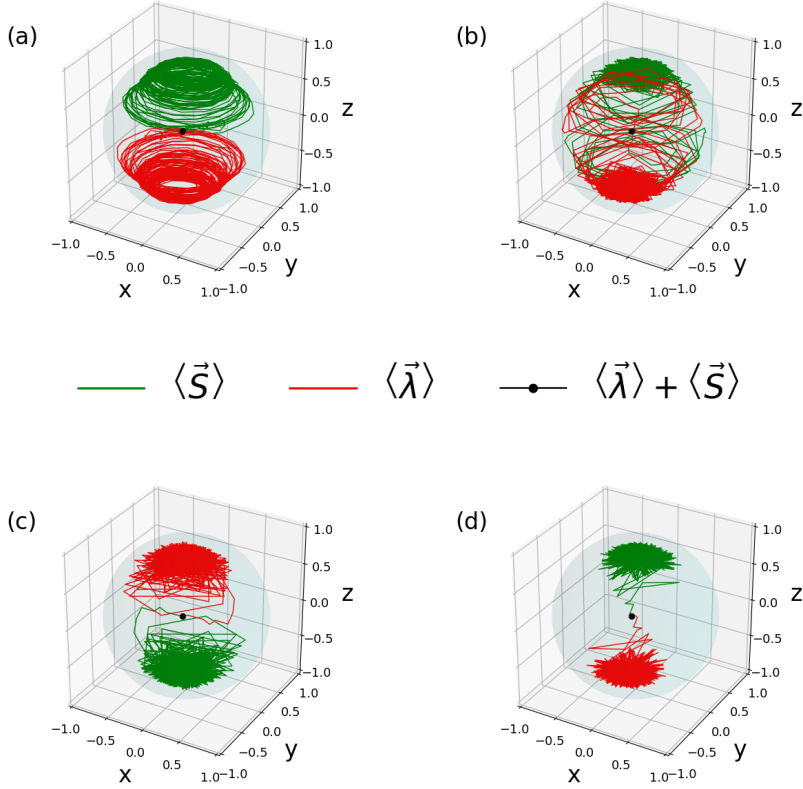


Figure 3: Conservation of total angular momentum for the full simulation duration and different values of the anisotropy coefficient C_2 : (a) 0.025, (b) 0.075, (c) 0.1, (d) 0.15 eV.Å². Total angular momentum (black) does not vary during the simulation, while the individual components, the average per atom spin (green curve) and lattice rotational moment (red curve) do vary. As the value of C_2 increases, the coordinates of the average per-atom spin and lattice angular momenta take less time to approach the long (z) axis of the spheroid via exchange of angular momentum. This is also evident from the values of the derivatives at $t = 0$ of the hyperbolic tangent fits to the absolute values of the spin and lattice angular momenta in Fig. 2.

In order to provide visual confirmation of the trend in Fig. 2 (b), we plot in Fig. 3 the time evolution of the coordinates of the per-atom average angular

momenta of the spins (green), lattice (red) and their sum (black) for a range of values of C_2 . Since the anisotropy is uniaxial in this work, the green and red traces tend to cluster near the z -axis, and with opposite signs. The symmetry of the spin Hamiltonian implies that there is no preferred final direction of the average per-atom spin and lattice angular momenta as long as they are mutually opposite and generally point along the cluster’s easy axis (z in this case). Therefore, randomly, either of the spin or the lattice rotational angular momentum can be oriented along the positive z axis (see e.g. the traces of Fig. 3 (c) vs the other three traces); it is the relative orientation of rotational versus spin angular momenta which is important, and which are always opposite and equal, conserving total angular momentum.

Finally, we note that, to our knowledge, the only previous SLD simulation we are aware of that reproduces the EdH effect (Ref. [9]) applies an external magnetic field of 50 Tesla throughout the entire demagnetization process of a free face-centered cubic Co cluster. Also, only the z components of the spin and lattice angular momenta are plotted in Ref. [9], casting doubt on whether *total* angular momentum is actually conserved in their EdH simulation. (An external field can induce a non-zero overall spin torque due to individual contributions not cancelling out in a pairwise manner.)

4. Conclusion

We have shown analytically that the dynamic many-body model of uniaxial anisotropy described in Ref. [17] conserves the total angular momentum and energy of the system. We also implemented this model in the spin-lattice dynamics code SPILADY [32], and also make the source code available online [46]. Our implementation reproduces the full Einstein–de Haas effect in an isolated iron nanoparticle, consistent with the conservation of total angular momentum by the model over a range of values of the magnetic anisotropy coefficient C_2 . The value of this coefficient not only determines the rate at which exchange between spin and rotational angular momenta occurs, but also how quickly the

angular momenta align parallel to the long axis of the nanoparticle for positive C_2 .

The advantage of the approach followed in this work, compared to other similar generally applicable semi-classical models, is that the realistic EAM potential is used to describe interactions between the atoms, allowing accurate reproduction of *ab-initio* free surface energies and defects. Another advantage is that the angular momentum exchange occurs in a very stable and consistent manner, with full spin-lattice relaxation occurring in agreement with previously reported times ~ 100 ps. Moreover, neglecting shape anisotropy, the difference in per-atom magnetic anisotropy energy between spin populations oriented at 90° to each other in the same frozen atomic configuration, yields order-of-magnitude agreement, at the lower range of the magnetic anisotropy interaction strength, C_2 , with previously reported tight-binding values for Fe nanoclusters of comparable size. The development of dynamic anisotropy models due to local symmetry breaking at finite temperatures is therefore crucial to modeling fast demagnetization processes.

Our implementation of anisotropy can be employed to study any single-element ferromagnetic system in which local coupling between spins and atoms cannot be ignored. It is also possible to extend this approach to multiple-element systems once SPILADY, the underlying spin-lattice dynamics code used in this implementation, makes provision for this capability. For this reason it is likely to find applications in a significant number of situations where uniaxial magnetization is important and coupling between lattice and spins plays a non-negligible role.

Acknowledgements

We acknowledge financial support from the Ministry of Science and Innovation of Spain (grant No. PID2019-109539GB-4). This work was supported by the Generalitat Valenciana through PROMETEO2017/139 and PROMETEO/2021/017. C. S. gratefully acknowledges financial supports from General-

itat Valenciana with (CDEIGENT2018/028). JFR acknowledges funding from FCT grant PTDC/FIS-MAC/2045/2021. The SLD calculations in this paper were performed on the high-performance computing facilities of the University of South Africa.

References

- [1] A. Einstein, W. Haas, Experimental proof of the existence of ampère's molecular currents, KNAW, Proceedings, 18 I, 1915, Amsterdam 18 I (1915) 696–711.
URL <http://www.dwc.knaw.nl/DL/publications/PU00012546.pdf>
- [2] S. J. Barnett, Magnetization by Rotation, Phys. Rev. 6 (1915) 239. doi:10.1103/PhysRev.6.239.
- [3] L. Landau, E. Lifshitz, L. Pitaevskii, Electrodynamics of Continuous Media, Course of Theoretical Physics, Butterworth-Heinemann, Oxford, 1995.
- [4] G. E. W. Bauer, S. Bretzel, A. Brataas, Y. Tserkovnyak, Nanoscale magnetic heat pumps and engines, Phys. Rev. B 81 (2010) 024427.
- [5] G. E. Bauer, E. Saitoh, B. J. V. Wees, Spin caloritronics, Nat. Mater. 11 (2012) 391.
- [6] K. Fukushima, S. Pu, Z. Qiu, Eddy magnetization from the chiral Barnett effect, Phys. Rev. A 99 (2019) 032105.
- [7] G. G. Scott, Review of gyromagnetic ratio experiments, Rev. Mod. Phys. 34 (1962) 102–109.
- [8] T. M. Wallis, J. Moreland, P. Kabos, Einsteinde Haas effect in a NiFe film deposited on a microcantilever, Appl. Phys. Lett. 89 (2006) 122502.
- [9] M. Afmann, U. Nowak, Spin-lattice relaxation beyond gilbert damping, J. Magn. Magn. 469 (2018) 217–223. doi:10.1016/j.jmmm.2018.08.034.

- [10] A. A. Kovalev, G. E. W. Bauer, A. Brataas, Current-driven ferromagnetic resonance, mechanical torques, and rotary motion in magnetic nanostructures, *Phys. Rev. B* 75 (2007) 014430.
- [11] R. Jaafar, E. M. Chudnovsky, D. A. Garanin, Dynamics of the Einstein-de Haas effect: Application to a magnetic cantilever, *Phys. Rev. B* 79 (2009) 104410.
- [12] E. M. Chudnovsky, D. A. Garanin, Rotational states of a nanomagnet, *Phys. Rev. B* 81 (2010) 214423.
- [13] J. H. Mentink, M. I. Katsnelson, M. Lemsheko, Quantum many-body dynamics of the Einstein-de Haas effect, *Phys. Rev. B* 99 (2019) 064428.
- [14] N. Bloembergen, S. Shapiro, P. Pershan, J. Artman, Cross-relaxation in spin systems, *Physical Review* 114 (2) (1959) 445.
- [15] D. Beaujouan, P. Thibaudeau, C. Barreateau, Anisotropic magnetic molecular dynamics of cobalt nanowires, *Phys. Rev. B* 86 (2012) 174409. doi:10.1103/PhysRevB.86.174409.
URL <https://journals.aps.org/prb/abstract/10.1103/PhysRevB.86.174409>
- [16] D. Perera, Atomistic simulations of magnetic models with coupled translational and spin degrees of freedom, Ph.D. thesis, University of Georgia (2015).
- [17] D. Perera, M. Eisenbach, D. M. Nicholson, G. M. Stocks, D. P. Landau, Reinventing atomistic magnetic simulations with spin-orbit coupling, *Phys. Rev. B* 93 (2016) 060402. doi:10.1103/PhysRevB.93.060402.
URL <https://doi.org/10.1103/PhysRevB.93.060402>
- [18] M. Aßmann, Atomistic simulation of spin-lattice dynamics, Ph.D. thesis, University of Konstanz (2018).

- [19] J. Hellsvik, D. Thonig, K. Modin, D. Iusan, A. Bergman, O. Eriksson, L. Bergqvist, A. Delin, General method for atomistic spin-lattice dynamics with first principles accuracy, *Phys. Rev. B* 99 (2018) 104302. doi:10.1103/PhysRevB.99.104302.
- [20] J. Tranchida, S. Plimpton, P. Thibaudeau, A. Thompson, Massively parallel symplectic algorithm for coupled magnetic spin dynamics and molecular dynamics, *J. Comp. Phys.* 372 (2018) 406–425. doi:10.1016/j.jcp.2018.06.042.
- [21] P. Nieves, J. Tranchida, S. Arapan, D. Legut, Spin-lattice model for cubic crystals, *Phys. Rev. B* 103 (2021) 094437. doi:10.1103/PhysRevB.103.094437.
URL <https://link.aps.org/doi/10.1103/PhysRevB.103.094437>
- [22] M. Strungaru, M. O. A. Ellis, S. Ruta, O. Chubykalo-Fesenko, R. F. L. Evans, R. W. Chantrell, Spin-lattice dynamics model with angular momentum transfer for canonical and microcanonical ensembles, *Phys. Rev. B* 103 (2) (2021) 1–13. doi:10.1103/physrevb.103.024429.
- [23] M. Eisenbach, D. Perera, D. P. Landau, D. M. Nicholson, J. Yin, G. Brown, Magnetic materials at finite temperatures: Thermodynamics and combined spin and molecular dynamics derived from first principles calculations, *J. Phys.: Conf. Ser.* 640 (2015) 012019.
- [24] W. Dednam, C. Sabater, O. Tal, J. J. Palacios, A. E. Botha, M. J. Caturla, Refined electron-spin transport model for single-element ferromagnetic systems: Application to nickel nanocontacts, *Phys. Rev. B* 102 (2020) 245415. doi:10.1103/PhysRevB.102.245415.
URL <https://link.aps.org/doi/10.1103/PhysRevB.102.245415>
- [25] J. M. Caridad, D. McCloskey, J. F. Donegan, V. Krstić, Controllable growth of metallic nano-helices at room temperature conditions, *Appl. Phys. Lett.* 105 (2014) 233114. doi:10.1063/1.4904091.

- [26] S. Finizio, M. Foerster, M. Buzzi, B. Krüger, M. Jourdan, C. A. F. Vaz, J. Hockel, T. Miyawaki, A. Tkach, S. Valencia, F. Kronast, G. P. Carman, F. Nolting, M. Kläui, Magnetic anisotropy engineering in thin film ni nanostructures by magnetoelastic coupling, *Phys. Rev. Applied* 1 (2014) 021001. doi:10.1103/PhysRevApplied.1.021001. URL <https://link.aps.org/doi/10.1103/PhysRevApplied.1.021001>
- [27] D. B. Reeves, J. B. Weaver, Approaches for modeling magnetic nanoparticle dynamics, *Critical Reviews in Biomedical Engineering* 42 (1) (2014) 85.
- [28] J.-Y. Chaulaeau, et al., Electric and antiferromagnetic chiral textures at multiferroic domain walls, *Nature Materials* 4 (2020) 386–390. doi:10.1038/s41563-019-0516-z.
- [29] A. Fert, N. Reyren, V. Cros, Magnetic skyrmions: advances in physics and potential applications, *Nature Reviews Materials* 2 (2017) 17031. doi:10.1038/natrevmats.2017.31.
- [30] J. Zázvorka, F. Jakobs, D. Heinze, N. Keil, S. Kromin, S. Jaiswal, K. Litzius, G. Jakob, P. Virnau, D. Pinna, K. Everschor-Sitte, L. Rózsa, A. Donges, U. Nowak, M. Kläui, Thermal skyrmion diffusion used in a reshuffler device, *Nature Nanotechnology* 14 (2019) 658–661. doi:10.1038/s41565-019-0436-8.
- [31] B. D. Cullity, C. D. Graham, *Introduction to magnetic materials*, 2nd Edition, Wiley, New Jersey, 2009.
- [32] P.-W. Ma, S. L. Dudarev, C. H. Woo, Spilady: A parallel cpu and gpu code for spinlattice magnetic molecular dynamics simulations, *Comp. Phys. Comm.* 207 (2016) 350 – 361. doi:<https://doi.org/10.1016/j.cpc.2016.05.017>.
- [33] P.-W. Ma, C. H. Woo, S. L. Dudarev, Large-scale simulation of the spinlattice dynamics in ferromagnetic iron, *Phys. Rev. B* 78 (2) (2008) 024434.

doi:10.1103/PhysRevB.78.024434.

URL <http://link.aps.org/doi/10.1103/PhysRevB.78.024434>

- [34] M. S. Daw, M. I. Baskes, Semiempirical, quantum mechanical calculation of hydrogen embrittlement in metals, *Phys. Rev. Lett.* 50 (17) (1983) 1285.
- [35] W. Dednam, Atomistic simulations of competing influences on electron transport across metal nanocontacts, Ph.D. thesis, University of Alicante/University of South Africa (2019).
- [36] M. Krech, A. Bunker, D. Landau, Fast spin dynamics algorithms for classical spin systems, *Comput. Phys. Commun.* 111 (1) (1998) 1–13. doi:10.1016/S0010-4655(98)00009-5.
- [37] D. P. Landau, S.-H. Tsai, M. Krech, A. Bunker, Improved spin dynamics simulations of magnetic excitations, *Int. J. Mod. Phys. C* 10 (08) (1999) 1541–1551.
- [38] C. Dornes, Y. Acremann, M. Savoini, M. Kubli, M. Neugebauer, E. Abreu, L. Huber, G. Lantz, C. Vaz, H. Lemke, E. Bothschafter, M. Porer, V. Esposito, L. Rettig, M. Buzzi, A. Alberca, Y. Windsor, P. Beaud, U. Staub, S. Johnson, The ultrafast einstein-de haas effect, *Nature* 565 (01 2019). doi:10.1038/s41586-018-0822-7.
- [39] E. Beaurepaire, J.-C. Merle, A. Daunois, J.-Y. Bigot, Ultrafast spin dynamics in ferromagnetic nickel, *Phys. Rev. Lett.* 76 (1996) 4250–4253. doi:10.1103/PhysRevLett.76.4250. URL <https://link.aps.org/doi/10.1103/PhysRevLett.76.4250>
- [40] P.-W. Ma, S. L. Dudarev, C. H. Woo, Spin-lattice-electron dynamics simulations of magnetic materials, *Phys. Rev. B* 85 (2012) 184301. doi:10.1103/PhysRevB.85.184301. URL <https://link.aps.org/doi/10.1103/PhysRevB.85.184301>
- [41] L. Malerba, M. C. Marinica, N. Anento, C. Björkas, H. Nguyen, C. Domain, F. Djurabekova, P. Olsson, K. Nordlund, A. Serra, D. Terentyev,

F. Willaime, C. S. Becquart, Comparison of empirical interatomic potentials for iron applied to radiation damage studies, *J. Nucl. Mater.* 406 (1) (2010) 19 – 38. doi:10.1016/j.jnucmat.2010.05.017.
URL <http://www.sciencedirect.com/science/article/pii/S0022311510002291>

- [42] D. Li, A. Smogunov, C. Barreteau, F. Ducastelle, D. Spanjaard, Magnetocrystalline anisotropy energy of Fe (001) and Fe (110) slabs and nanoclusters: A detailed local analysis within a tight-binding model, *Physical Review B* 88 (21) (2013) 1–9. doi:10.1103/PhysRevB.88.214413.
- [43] W. B. Nurdin, K.-D. Schotte, Dynamical temperature for spin systems, *Phys. Rev. E* 61 (2000) 3579–3582. doi:10.1103/PhysRevE.61.3579.
URL <https://link.aps.org/doi/10.1103/PhysRevE.61.3579>
- [44] G. Dos Santos, R. Aparicio, D. Linares, E. N. Miranda, J. Tranchida, G. M. Pastor, E. M. Bringa, Size- and temperature-dependent magnetization of iron nanoclusters, *Phys. Rev. B* 102 (2020) 184426. doi:10.1103/PhysRevB.102.184426.
URL <https://link.aps.org/doi/10.1103/PhysRevB.102.184426>
- [45] G. Dos Santos, R. Meyer, R. Aparicio, J. Tranchida, E. M. Bringa, H. M. Urbassek, Spin-lattice dynamics of surface vs core magnetization in Fe nanoparticles, *Applied Physics Letters* 119 (16) (2021) 012404. doi:10.1063/5.0055606.
URL <https://aip.scitation.org/doi/10.1063/5.0055606>
- [46] P.-W. Ma, et al., computer code SPILADY, with anisotropy corrections made by W. Dednam (2018).
URL <https://github.com/wdednam/spilady/tree/anisotropy>